SSRG International Journal of Electrical and Electronics Engineering
ISSN: 2348-8379/ https://doi.org/10.14445/23488379/IJEEE-V11I6P132

Volume 11 Issue 6, 317-329, June 2024

Original Article

Hybrid Energy Optimization for Reliable Water Pumping System: Integrating PV, Wind, and BLDC Motor with Advanced Control Strategies

P. Nagendra[1], K. Sasikala[2]

[1,2]*Department of EEE, School of Engineering, Vels Institute of Science Technology & Advanced Studies, Tamilnadu, India.*

[1]*Corresponding Author : pathakotlanagendra@gmail.com*

Received: 15 April 2024 Revised: 17 May 2024 Accepted: 15 June 2024 Published: 29 June 2024

Abstract - *The improved pumping system reliability makes it possible to fully utilize a PV array, wind, and motor pump. This paper provides a new optimization strategy for a hybrid energy system that combines wind and grid-controlled Photovoltaic (PV) power with a Brushless DC (BLDC) engine to power a pump for water. The proposed strategy combines the use of Giant Trevally Optimization (GTO) for step size optimization with an Incremental Conductance-Giant Trevally Optimization (INC-GTO) Maximum Power Point Tracking (MPPT) algorithm. A powerful Zeta converter is employed in the setup to convert energy for the PV water drive usage, which is provided by a BLDC. The energy flow from the PV array, wind, and grid is managed by an Optimized Fuzzy-Fractional Order Proportional-Integral-Derivative (O-FFOPID) Controller that is optimized via GTO. It dynamically modifies the speed and power consumption of the BLDC motor in response to variations in the water demand and environmental conditions. The controller adapts to changing load demands and environmental conditions with ease by taking into account the dynamic nature of solar resources. The study illustrates the attainment of maximum power point operation for the power quality improvements and PV array, including a decrease in Total Harmonic Distortion (THD) in the network and power factor correction using Matlab/Simulink simulations. Maximizing energy extraction and improving system sustainability are the goals of integrating renewable energy sources. This research improves the efficiency and dependability of water pumping systems while advancing the use of renewable energy sources.*

Keywords - *Water pumping, Brushless DC (BLDC) motor, Incremental Conductance-Giant Trevally Optimization (INC-GTO), Optimized Fuzzy-Fractional Order Proportional-Integral-Derivative (O-FFOPID), MPPT, THD.*

1. Introduction

Water resources are essential for social and economic development, as well as for meeting human needs, ensuring food production, and safeguarding health. Water pumping is typically dependent on electricity generated by diesel engines across the globe [1]. Worldwide, irrigation is used at different levels and is a well-established practice on many farms. The constant rise in carbon releases and the depletion of fossil fuels push consumers to switch to renewable sources right away [2].

In the rural areas of many developing nations, diesel is costly and hard to come by. If it is, it can be challenging to deliver to isolated locations. Among the potential uses of photovoltaic energy are pumping systems, which are especially useful in remote locations with high levels of insolation and no connection to the electrical grid [3]. Then, a motor and PV, a DC/DC converter make up our system, which provides energy to the pump [4]. The use of photovoltaic sources has several advantages, including being a sustainable and free fuel source, being lightweight even though PV systems can cover large areas, operating silently because there is no large rotating machinery, being able to be installed close to the point of use, being easy to install, having predictable availability in some areas, and requiring relatively little routine maintenance [5].

The greatest substitute for traditional sources for a variety of appliances is turning out to be solar Photovoltaic (PV) generation. One important PV energy application that has attracted much attention recently is water pumping [6]. Over the past ten years, permanent magnet Brushless DC (BLDC) motors have become more and more popular because of their high power density, low maintenance requirements, extended lifespan, minimal Electromagnetic Interference (EMI), and compact design [7]. The introduction of this motor has been found to improve performance and provide maintenance-free operation while also lowering the cost and size of PV panels. One of the main problems with solar PV generation is its intermittency, which leads to an unreliable water pumping system [8].

Adverse weather conditions cause major disruptions to the flow of water, and because the pump is not operating at peak efficiency, the system is not fully utilized. Moreover, the water pumping system shuts down when there is no sunlight present at night. It will take overcoming these shortcomings to obtain a dependable PV-based pumping system [9]. To attain optimal PV module usage, a suitable algorithm-equipped MPPT device is necessary to generate the optimum quantity of energy from the PV structure. However, adding a second device to trail the extreme energy will boost the system's dimensions and design [10].

BLDC motors are more energy-efficient than asynchronous motors and have higher torque/inertia ratios, power densities, efficiency, and power factors; they are significant contributors to this problem [11]. Many applications, such as water pumping, have switched from asynchronous motors to this one. The utilization of transducer models like Zeta converters and positively Interleaved Luo converters (I-Luo) maximizes the functioning energy from the SPV array by decreasing switching losses and enhancing output [12]**.**

The PV array's power transmission can be optimized with a BLDC motor, which also improves the pumping system's dependability [13]. Maintenance is necessary for the DC motor-based pumping system due to the existence of commutators and brushes. DC motors are, therefore, rarely employed in PV pumping applications. Single-phase induction motors have also driven low-inertia torque loads. The induction motors' complicated control scheme renders them ineffective for pumping applications [14].

As a result, in this study, Brushless DC (BLDC) motors have been taken into consideration because they require less maintenance than AC motors and have a low power range and straightforward design control [15].

The major contributions of this work are,

- Incorporating the MPPT algorithm of INC-GTO for effective PV array power management. This algorithm maximizes the extraction of energy from solar resources by dynamically adjusting the PV array's functioning point to track the MPP.
- The PV array, wind turbine, and grid power flow are managed by an O-FFOPID controller that is optimized via GTO. This advanced control strategy dynamically adjusts the BLDC motor speed and power consumption in response to changing environmental conditions.
- The O-FFOPID controller takes into account the dynamic nature of solar resources to adjust to changes in load demands and environmental conditions. By ensuring smooth system operation in a variety of scenarios, this adaptive control mechanism further improves the system's sustainability and dependability.

The structure of the paper is as follows: Section 2 represents a review of the relevant works. Section 3 delves into the proposed method, and Section 4 deliberateson the obtained outcomes. Lastly, Section 5 completes the paper.

2. Literature Survey

In the literature survey, various studies have explored the application of renewable sources in optimizing the performance of grid-controlled BLDC motor-based water pumping systems. Kishore and Prashanth (2022) [16] have suggested a grid-interactive solar photovoltaic-fed water-propelling model with bidirectional power flow. To run a water pump, a BLDC motor drivewas used without phase current. When water pumping was not necessary, this system allowed users to initiate a single-phase utility grid and run the water pump at maximum ability for 24 hours a day, despite the weather.

Satyanarayana and Kumar (2021) [17] have provided a fuzzy controller-based method for a BLDC that is fed by a single array and is used to pump water in applications. The fuzzy-based MPPT was discovered to produce better outcomes than other methods when it came to randomly varying atmospheric conditions. MPPT techniques were employed to derive the MPP from a PV module. The Landsman converter was the only DC-DC converter that could match the required performance for the suggested model. To illustrate the uniqueness of the suggested system, the SPV array-fed BLDC motor-driven steady-state, dynamic starting manners were shown.

Miqoi et al. (2019) [18] have offered the idea of the MPPT to accomplish this. The application of sliding mode control and its reliability and durability in non-linear systems were then the main topics of the article; however, it was pointed out that chattering phenomena represented a drawback. To improve control and adjust the switching gain, the article suggested using adaptive fuzzy sliding mode control, or AFSMC. To verify its effectiveness, the AFSMC was contrasted with the Sliding Mode Controller (SMC) and the perturb and observe technique.

Wang et al. (2022) [19] have improved the Brushless DC Motor's (BLDCM) capacity for speed control by suggesting an innovative Proportion Integration Differentiation (PID). They used Harmony Search Algorithm (HSA) optimization with dual Fuzzy Logic Systems (FLSs), or DFPID-HSA. At first, FLS1 in DFPID-HSA locked the PID controller's three coefficients over a wide range depending on the error change rate and system error.

Subsequently, FLS2 underwent HSA (HSA-F2) optimization to obtain accurate three-coefficient corrections. They employed an enhanced dynamic adjustment mode for the distance Bandwidth (BW) and Pitch Adjustment Rate (PAR)

in HSA to maximize the improvement of global harmony. To aid in global search, they also used a triple selection approach in the composition harmony section.

Shokri et al. (2019) [20] have examined the operation of the solar water pumping model that is directly coupled under various solar radiation, temperature, and speed settings. Because of the high efficiency and small size of this drive, they used a BLDC engine to power a centrifugal drive that was attached to its shaft. The effectiveness of the water pumping system's transient and steady-state response was represented by MATLAB software, which was also used for the system's design, analysis, and control.

Shchur et al. (2021) [21] have integrated external power supply, battery storage, and both general and local control functions for the PV pumping model into a Passivity Based Control (PBC) system. Due to the way the EMS was built, only 2 PBC schemes were created for all manners. Two Control Influence Former (CIF) frameworks were created for each system, and computer simulation was used to study how each one worked. The control system enabled the necessary power regulation, even though the implementation of CIFs was made simple by the interconnection and damping coefficients that were introduced.

De Oliveira Ferreira et al. (2020) [22] have suggested, created a computational model, and examined a small hybrid PV-wind water pumping. The Multi-Input DC-DC Converter (MIC) in the suggested approach connected the energy sources, and its output did not require a battery bank because it was directly connected to a DC motor pump.

To operate the sources at chosen points on their characteristic curves, the MIC operated on their drained currents either simultaneously or separately. The simulations showed that the system operated well, suggesting that it could be used in remote areas and that it could be put into practice.

Bakır et al. (2023) [23] have offered the control and modeling for an efficient hybrid water pumping system that makes use of a brushless DC motor. To achieve effective water pumping, the system included PV and battery. The battery's operating modes were automatically switched between with the use of a bi-directional charge control mechanism and a buck-boost converter. The water cycle optimization's performance was assessed by contrasting it with alternative approaches based on settling time and overshoot values, demonstrating its potency in result analysis.

Shukla and Singh (2020) [24] have examined an integrated photovoltaic-grid system that ran a water pump via an Induction Motor (IM). A modified Space Vector Modulation (SVM) technique was applied to estimate the phase currents of induction engines from the DC-link current. A model reference adaptive system based on artificial neural networks was utilized in this system to estimate speed. An IM pump was controlled for speed using field-oriented control.

Ramakrishna and Kumar (2023) [25] have recommended the bidirectional control of power flow in a grid-interacting water pumping model that PV feeds. A single-phase Voltage Source Converter fed a BLDC motor, controlling power flow in both directions between the DC bus of the voltage source inverter and the grid via an ANFIS-based Unit Vector Template (UVT) generation method. Switching loss was decreased by operating the VSI at a fundamental frequency.

2.1. Problem Statement

The studies included in the literature review aim to solve the problem of maximizing the efficiency of water pumping systems that use grid-controlled BLDC motor-based configurations that are powered by renewable energy, specifically solar PV and wind. These systems are designed to maximize energy extraction and system efficiency while overcoming obstacles like changing environmental conditions, load demands, and power quality issues. To dynamically adjust motor speed and power consumption based on system dynamics, several strategies have been investigated, including the integration of advanced control strategies like fuzzy logic, FOPID control, and sliding mode control. To further increase system performance and reliability, the research also focuses on optimizing power flow control, power factor correction, and lowering THD in grid-interfaced solutions. Effective MPPT algorithms designed for nonlinear systems are also discussed, as well as issues like the chattering phenomenon in sliding mode control. Furthermore, innovative control algorithms for bidirectional power flow control and the incorporation of energy storage solutions, like battery banks, help to address the dependability and effectiveness of hybrid water pumping systems.

3. Proposed Methodology

This research grants a fresh method to enhance the performance of a water pumping system with a grid-controlled Photovoltaic (PV) and Wind hybrid energy source coupled with the BLDC motor. The proposed control scheme is based on the INC-Giant Trevally Optimization (GTO) MPPT algorithm. The step size of INC-MPPT is optimized using the GTO. This paper construes the Zeta converter-occupied BLDC-directed PV water pump application. The integration of renewable energy sources aims to enhance the scheme's sustainability and efficiency.

An O-FFOPID is implemented to intelligently manage the energy flow from the PV array, wind turbine, and electrical grid, ensuring optimal utilization of available energy. The Fuzzy-FOPID is optimized using the GTO. Moreover, Fuzzy controller design has taken into consideration sigmoidal membership functions. The Fuzzy-FOPID Controller takes into account the dynamic nature of solar resources, along with

varying water demand, to dynamically adjust the BLDC motor speed and power consumption. This adaptive control strategy enables the system to operate seamlessly across different environmental conditions and load demands, maximizing energy extraction from renewable sources. Figure 1 illustrates the overall control strategy of a hybrid water pumping system.

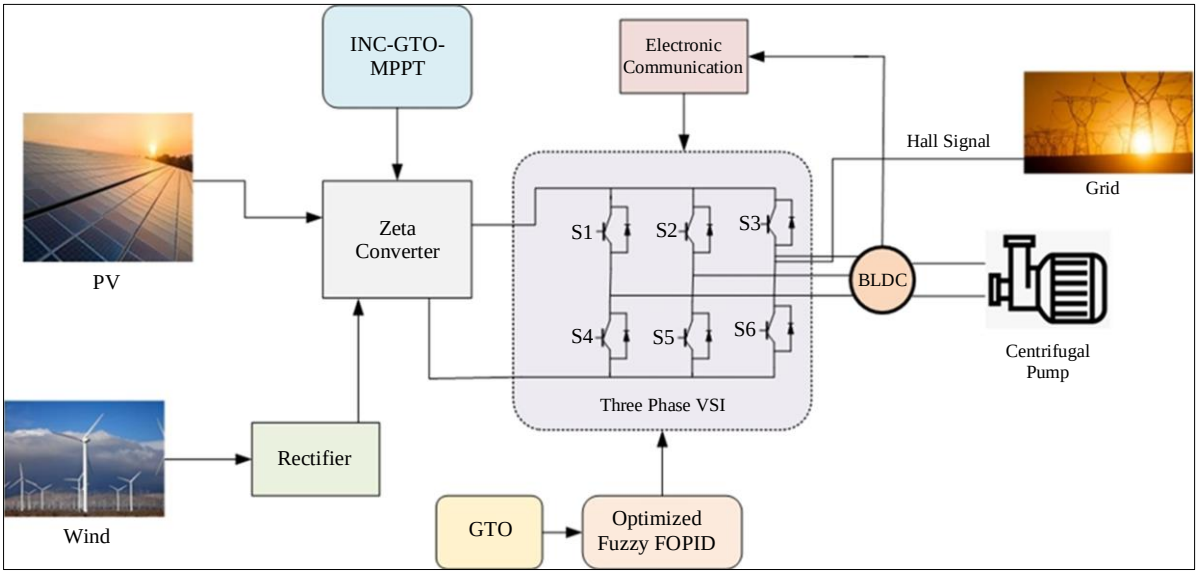

Fig. 1 The overall control strategy of the water pumping system

3.1. PV Modelling

Figure 2 presents a very fundamental mathematical representation of the Photovoltaic cell's one-diode model, which also shows the effects of environmental factors and non-linear characteristics. The expression for the photovoltaic output current is,

$$I_{pv} = I_{photon} - I_{diode} - I_{shunt} \quad (1)$$

The linear V-I characteristics of a photovoltaic cell can be obtained mathematically as follows:

$$V_{pv} = \frac{1}{\lambda_{constant}} \ln\left(\frac{I_{pv\_sc} - I_{pv} + I_{rs}}{I_{rs}}\right) - R_{series} I_{pv} \quad (2)$$

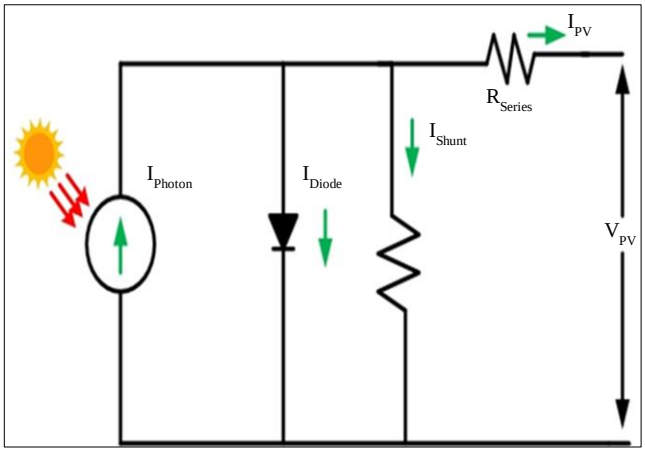

Fig. 2 Equivalent circuit of PV

3.2. Wind Turbine Modelling

Wind energy is transformed into mechanical output by a wind turbine. The extracted mechanical output with wind velocity can be expressed mathematically as (3),

$$P_w = \frac{1}{2} C_{p.c} \delta_{ad} R_t^2 V_{wd}^3 \quad (3)$$

The characteristics of pitch blade angle (β or β_{pb}) and tip speed (λ) determine the wind turbine performance coefficient and explain the conversion losses. The relation attained mathematically is given below,

$$C_{p.c}(\lambda\beta) = K_1 \left(\frac{K_2}{\lambda_i} - K_3\beta - K_4\right) e^{\frac{K_5}{\lambda_i}} + K_6\lambda \quad (4)$$

$$\lambda = \frac{\omega_T * R_t}{V_{wd}}, \frac{1}{\lambda_i} = \frac{1}{\lambda + 0.08} - \frac{0.0035}{1+\beta^2} \quad (5)$$

The turbine coefficients denoted by variables K1 through K6 are different for wind turbines with variable and constant velocities. Additionally, the tip speed ratio (λ) shows the proportion between a wind turbine's angular velocity and wind velocity. The pitch angle (β) indicates the angle at which the turbine's blades align with the longitudinal axis.

3.2.1. BLDC Motor Mathematical Model

The following presumptions apply to the mathematical model: The armature winding is balanced; the armature winding's active resistance is constant; Losses in magnetic saturation and steel are not taken into account. Therefore, the

equilibrium powers in the armature winding's 3-phase circuits are described by the vector-matrix equation.

$$\vec{v} = R\vec{\imath} + L\frac{d}{dt}\vec{\imath} + \vec{e} \quad (6)$$

Where the $\vec{v}$are the vector columns of the phase back-EMFs, voltages, and currents, and 3 similar active resistances arranged diagonally are represented by R, and $\vec{e}$, $\vec{\imath}$correspondingly. Mutual interphase inductances M are used to fill in the remaining cells, while$R$ is the phase windings and L is the matrix formed diagonally by the phase winding self-inductances.

Since there are no currents in any of the machine's three star-connected phases, the BLDC motor's dynamic equations acquired from Equation (7) can be stated in matrix form as follows.

$$\begin{bmatrix} v_a \\ v_b \\ v_c \end{bmatrix} = \begin{bmatrix} R & 0 & 0 \\ 0 & R & 0 \\ 0 & 0 & R \end{bmatrix} \begin{bmatrix} i_a \\ i_b \\ i_c \end{bmatrix} + \begin{bmatrix} L-M & 0 & 0 \\ 0 & L-M & 0 \\ 0 & 0 & L-M \end{bmatrix} \frac{d}{dt} \begin{bmatrix} i_a \\ i_b \\ i_c \end{bmatrix} + \begin{bmatrix} e_a \\ e_b \\ e_c \end{bmatrix} \quad (7)$$

The following should be the back-EMFs for each phase in Equation (8):

$$e_a = K_\omega f(\theta_e), e_b = K_\omega f(\theta_e - 120^\circ)\omega, e_c = K_\omega f(\theta_e - 240^\circ)\omega \quad (8)$$

Where, K_ω is the back-EMF constant,ω is the motor's angular velocity, θ_e and is the rotor angle.

$$\theta_e = p\theta_m = p\int \omega \; dt \quad (9)$$

The function provides the trapezoidal waveform $f(\theta_e)$, and one period of this function can be expressed as

$$f(\theta_e) = \begin{cases} 1 & if \quad 0 \le \theta_e < \frac{2\pi}{3} \\ 1 - \frac{\pi}{6}\left(\theta_e - \frac{2\pi}{3}\right) & if \quad \frac{2\pi}{3} \le \theta_e < \pi \\ 1 & if \quad \pi \le \theta_e < \frac{5\pi}{3} \\ -1 + \frac{\pi}{6}\left(\theta_e + \frac{2\pi}{3}\right) & if \quad \frac{5\pi}{3} \le \theta_e < 2\pi \end{cases} \quad (10)$$

The following formula provides the motor's electromagnetic torque:

$$T_e = \frac{(\vec{e}.\vec{\imath})}{\omega} \quad (11)$$

The dot product of the armature current vector and the back-EMF is represented by the symbol $(\vec{e}.\vec{\imath})$. The equation of motion for a single-mass mechanical drive model has the following form when the motor shaft is the only source of the total moment of inertia (J_Σ).

$$J_\Sigma \frac{d\omega}{dt} = T_e - T_L - B_\omega \quad (12)$$

Where B is the dumping coefficient and T_L is the drive's load torque.

A 3-phase VSI powers the BLDCM with a 6-step commutation order. 3 integrated, low-cost hall sensors produce three logic signals, h_1, h_2, and h_3 based on the position of the rotor. A decoder circuit then translates these signals into the six switching pulses, S1-S6, that are needed to operate the VSI. To decrease conduction losses, only 2 switches are active at a time. The BLDCM's electronic commutation was done at fundamental frequency switching to reduce further the number of losses in the motor and VSI.

3.3. Centrifugal Pump Mathematical Model

An example of a hydrodynamic load is the centrifugal pump. Next, the following Equation (13) describes the torque and power of the load:

$$P_{cp} = k_\omega \omega^3, T_{cp} = k_\omega \omega^2 \quad (13)$$

Where, k_ω is the pump load constant.

3.4. Incremental Conductance-Giant Trevally Optimization MPPT

One of the most widely used MPP algorithms is the INC algorithm. The movement toward the MPP is determined by the PV's conductance, which gives rise to the method's name. The PV module output is used to measure the current and voltage. The INC-GTO MPPT algorithm adapts its operating point dynamically to track the MPP in a variety of environmental conditions, exploiting the energy output of a PV.

The INC-GTO algorithm detects changes in the PV array's energy yield by continuously measuring its voltage and current output and gradually adjusting the operating voltage. The algorithm determines which direction the operating voltage should be adjusted to approach the MPP by contrasting the instantaneous power output with the preceding value.

The derivative of current in voltage is calculated using the values of the changes in voltage and current. Moreover, the traditional INC algorithm is based on comparing the PV array's instantaneous current against voltage and its derivative as a function of voltage. This algorithm monitors the MPP by varying the reference voltage according to the system's operating point. The following requirements must be fulfilled at MPP:

$$\frac{dP}{dV} = 0 \tag{14}$$

$$\frac{dP}{dV} = \frac{d(V.I)}{dV} = I\frac{dV}{dV} + V\frac{dI}{dV} \tag{15}$$

$$\frac{dI}{dV} = -\frac{I}{V} \tag{16}$$

Where, I/V is the PV instantaneous current and dI/dV is the derivative of current as a function of voltage. Additionally, the reference voltage is increased depending on a fixed step voltage if dI/dV>0. Meanwhile, based on the fixed step voltage, the reference voltage decreases if dI/dV<0. The performance of this algorithm depends critically on the step size.

3.5. Giant Trevally Optimization for Step Size Optimization

The GTO technique is then applied to optimize the step size used in the adjustment process. The giant trevally fish, which is renowned for its effective hunting techniques, served as the model for the GTO algorithm, a metaheuristic optimization technique. GTO is used to find the most optimal step size that maximizes the power abstraction from the PV array in the context of optimizing the step size in the INC-MPPT algorithm.

This guarantees that the algorithm can quickly and precisely monitor changes in the surrounding environment and modify the PV array's operating point to optimize power output. The giant trevally's hunting habits serve as the model for the GTO technique, a metaheuristic algorithm. The giant trevally employs strategies such as jumping out of the water to catch prey, choosing an ideal hunting area, and patterning its foraging movements. These tactics are replicated by the GTO algorithm in a three-step process: thorough search, area selection, and attack.

3.5.1. Extensive Search

The GTO method uses a mathematical model based on Levy flights, a type of random walk, to simulate the great distances giant trevallies travel in search of food. This stage helps the algorithm avoid local optima and enhances its exploration capabilities. The following illustration provides an example of the equation used in this phase:

$$X(t+1) = Best_p \times R + (Maximum - Minimum) \times R + Minimum \times levy(Dim) \tag{17}$$

Where $Best_p$ indicates the best location achieved, R denotes a random number between 0 and 1, $levy(Dim)$signifies the levy flight, and $X(t+1)$ is the giant trevally's location vector in the subsequent iteration. $levy(Dim)$ refers to the levy flight, a unique category of non-Gaussian stochastic processes, where the Levy distribution dictates the phase scopes.

The procedure's capacity to conduct a globalexploration is facilitated by sporadic large steps. Moreover, avoiding local optima and accelerating the rate of convergence are the primary benefits of employing Levy flight. $levy(Dim)$ should be computed with (17):

$$levy(Dim) = step \times \frac{u \times \sigma}{|v|^{\frac{1}{\beta}}} \tag{18}$$

Where u and v are random numbers normally dispersed in the range (0; 1),$step$ is the step size, which is fixed at 0.01, and β is the index of the levy flight distribution function, which can take values ranging from 0 to 2 and has been set to 1.5. The σ is expressed as per the Equation (19):

$$\sigma = \left(\frac{\Gamma(1+\beta) \times \sin\left(\frac{\pi\beta}{2}\right)}{\Gamma\left(\frac{1+\beta}{2}\right) \times \beta \times 2^{\left(\frac{\beta-1}{2}\right)}} \right) \tag{19}$$

3.5.2. Selecting an Area

During this stage, the system determines the best hunting area within the search space by looking at the availability of food. This behavior can be mathematically replicated using the following equation:

$$X(t+1) = Best_p \times \mathcal{A} \times R + Mean\_Info - X_i(t) \times R \tag{20}$$

Where $X_i(t)$ represents the current location, $\mathcal{A}$ is a parameter that controls position change, and R is a random integer. The giant trevallies have made use of every piece of knowledge from the previous points, as indicated by $Mean\_Info$ the mean, which can be computed using (21).

$$Mean\_Info = \frac{1}{N}\sum_{i=1}^{N} X_i(t) \tag{21}$$

Using 10 solutions (search agents) and five iterations, the Sphere function was used to assess the efficacy of the choosing area step.

3.5.3. Attacking

The final phase of the algorithm replicates the trevally's assault on its victim. To replicate the actions of a massive trevally while it chases and attacks its prey, GTO assumed that trevallies experience visual distortion, primarily due to light refraction. The trevally's behavior is affected by light refraction, which also affects its vision.

The algorithm uses Snell's equation to compute the visual distortion V, which it then uses to simulate the trevally attack. Snell's law states that at the point of refraction, the incident and refracted rays must both make an angle with the surface normal. The surface through which light beams are passing through is another crucial consideration. Snell's Law uses refractive indices, which have set values for particular media,

to demonstrate this relationship. Here, the angle of incidence can be employed to forecast the angle of refraction and vice versa. The Snell's law is illustrated in (22) below.

$$\eta_1 sin\theta_1 = \eta_2 sin\theta_2 \quad (22)$$

θ_1 and θ_2, respectively, represent the angles of incidence and refraction. A random number in the range [0, 360] is denoted by θ_2. From (22) θ_1 can be calculated using below (23):

$$sin\theta_1 = \frac{\eta_2}{\eta_1} sin\theta_2 \quad (23)$$

Next, (24) can be used to calculate the visual distortion $\mathcal{V}$:

$$\mathcal{V} = sin(\theta_1^{\circ}) \times \mathcal{D} \quad (24)$$

Where sin is the sine of a variable in degrees. The distance $\mathcal{D}$, which can be calculated using Equation (25) between the attacker and the prey:

$$\mathcal{D} = |(Best_P - X_i(t))| \quad (25)$$

Where $Best_P$, which represents the prey's location, is the best solution found thus far. Subsequently, utilizing (13), a mathematical simulation is employed to mimic the actions of giant trevally when they dive and leap from the water.

$$X(t+1) = \mathcal{L} + \mathcal{V} + \mathcal{H} \quad (26)$$

Where $\mathcal{H}$ is the function for the leaping slope, $\mathcal{V}$ is the visual distortion $\mathcal{L}$ is the launch speed, and $X(t+1)$indicates the next position. As a result, the algorithm may proceed from the exploration phase to the exploitation phase. $\mathcal{L}$, is used to mimic chasing the bird, can be computed using (27):

$$\mathcal{L} = X_i(t) \times sin(\theta_2^{\circ}) \times F_{obj} X_i(t) \quad (27)$$

Where the fitness value of X at iteration t is denoted by $F_{obj}X_i(t)$. The last term $\mathcal{H}$in (26) specifies the jumping slope function that enables the procedure to carry out a suitable transition between the exploitation and exploration stage adaptively and can be computed using (28):

$$\mathcal{H} = R \times (2 - t \times \frac{2}{T}) \quad (28)$$

Where T and t stand for the maximum number of iterations and the current iteration correspondingly. The efficiency of power extraction from the PV array is improved by incorporating the INC-GTO MPPT algorithm with the GTO optimization technique. This leads to an increase in energy yield from the renewable energy source and an improvement in overall performance. This helps to optimize the performance of the water pumping system and improve its sustainability by allowing the system to make the best use of the solar energy that is obtainable and to optimize the output of the PV array. The step size adjustment method is guaranteed to be optimized through the integration of GTO optimization, which improves system performance by enabling quicker and more accurate adjustments in response to changes in the environment.

3.6. Zeta Converter

Taking the MPP in the PV module, the INC-MPPT MPPT algorithm was used in this work. To improve overall system performance and efficiency, a BLDC motor and zeta converter are integrated into a PV-wind water pump application. This is a calculated move. An essential bridge that makes effective power conversion and utilization possible between the BLDCmotor and PV array is the zeta converter.

As a DC-DC converter, the zeta converter offers the voltage regulation and conversion abilities required to match the voltage levels between the BLDC and PV array. The equivalent circuit of the zeta converter is depicted in Figure 3.

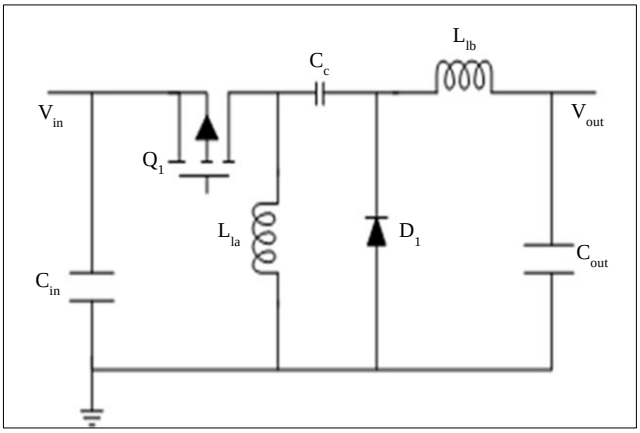

Fig. 3 Zeta converter's equivalent circuit

The energy source for the converter is a PV module. The MPPT algorithm will receive simultaneous measurements of the PV module's current and voltage. To generate the MPP from the PV power input, the duty cycle will be modified following the measurement of the input parameters. Pulse width modulation is produced by the duty cycle and delivered to the zeta converter to regulate the switching frequency. The appropriate energy is subsequently provided to the load through the converter by its output.

A zeta converter consists of two diodes, two inductors, and two capacitors. This fourth-order converter depends on a buck converter, which can operate in a step-down or step-up manner depending on the duty cycle of the switch employed in the circuit. 50 kHz is taken to be the rate of switching in the design. Equation (29) describes the value of each inductor.

$$L_{1a\ min} = L_{1b\ min} = V_{in}\left(\frac{D}{f_{sw}\times\Delta I_{L1a}}\right) \quad (29)$$

10% of the PV panel's input voltage is expected to be the ripple voltage of the input and series capacitors. As a result, Equation (30) describes the capacitance.

$$C_{in} = C_c = \frac{D\times I_{out}}{\Delta V\times f_{sw}} \quad (30)$$

However, Equation (31) determines the capacitance of the output capacitor.

$$C_{out} = \frac{\Delta I_{L1b}}{8\times\Delta V_{C_{out}}\times f_{sw}} \quad (31)$$

Where C is the capacitance of the capacitor, D is the duty cycle, ΔI_{L1a} and ΔI_{L1b} are the ripple current and voltage across the inductor, and $f_{sw} = \frac{1}{T}$ is the switching frequency. The system's power flow can be better controlled due to the zeta converter's integration.

The zeta converter allows for precise control over the speed and working of the BLDC motor, ensuring that it runs at its maximum efficiency under a variety of operating conditions. It does this by controlling the voltage levels and managing the power transfer.

3.7. Optimized Fuzzy Fractional Order PID Controller

The PV array, wind turbine, and electrical grid are just a few of the energy sources that the Optimized Fuzzy-FOPID (O-FFOPID) controller uses to efficiently accomplish the control flow to the BLDC motor in the water pumping system. This controller dynamically modifies the BLDC motor's power and speed consumption in response to shifting water demands and environmental changes by combining fuzzy logic, FOPID control, and optimization techniques.

FOPID controller and rule-based fuzzy logic control are combined to create the fuzzy fractional order PID controller. The fuzzy set model with a rule base allows for greater flexibility in system design and the clear linguistic notation of observations. The basis of operation for traditional controllers, such as fractional-order controllers, is the input of errors for the derivative, integral and proportional terms, each with a specified gain value.

As a result, for a complex and nonlinear system, the controller performance falls short of expectations. An attempt could be made to replace the fixed gain with a dynamic gain value for the derivative, proportional and integral terms. Enhancing controller presentation and rapidly achieving stable system output during external disturbances and load variation can be achieved by dynamically adjusting the gain in a FOPID structure.

Additionally, the fuzzy logic system outperforms other systems when it comes to fine-tuning the controller constraints in closed-loop control systems, especially those with nonlinear inputs and outputs. The gain parameters of the FOPID controller K_P, K_I and $K_D$are adjusted online in the proposed control structure in response to system dynamics.

In this control strategy, the controller gains $\Delta K_P, \Delta K_I$, and ΔK_D is obtained using a rule base by designing change-in-error inputs and a fuzzy logic controller with error. During every sampling period, the FOPID controller block updates the controller gain magnitude based on the inputs. Figure 4 depicts the typical FFOPID control structure's frame.

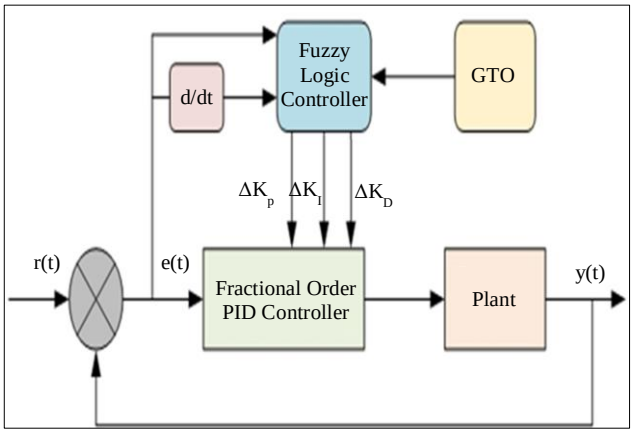

Fig. 4 Optimized FFOPID

The FFOPID control scheme's online gain modification will ensure the system's good dynamic and static characteristics even when the load varies and set-point conditions change. The FFOPID controller's final values for k_P, k_I, and k_D are provided in (32).

$$k_P = K_P + \Delta K_P$$
$$k_I = K_I + \Delta K_I \quad (32)$$
$$k_D = K_D + \Delta K_D$$

This work applies a Mamdani-type fuzzy inference system and uses sigmoidal connection purposes to more accurately and precisely represent the relationships between inputs and outputs. Five association roles are preferred for the outputs to generate exact outputs, while 3 connection roles are nominated for the inputs.

The linguistic variables that stand for negative small, Negative Big, Negative, Zero, Positive, Positive Big, and Positive Small, respectively, are NB, NS, N, Z, P, PS, and PB. To find the crisp output, the center of gravity defuzzification method is chosen. The fuzzy linguistic rule base is depicted in Table 1(a), (b), and (c).

Table 1(a). Fuzzy linguistic rule for K_P

ΔK_P		Δe		
		N	P	Z
e	N	NB	Z	NS
	Z	NB	NS	NB
	P	NS	PS	Z

Table 1(b). Fuzzy linguistic rule for K_D

ΔK_D		Δe		
		N	P	Z
e	N	NB	NS	NS
	Z	Z	PS	Z
	P	Z	PS	PS

Table 1(c). Fuzzy linguistic rule for K_I

ΔK_I		Δe		
		N	P	Z
e	N	NB	NS	NS
	Z	NS	PS	Z
	P	Z	PB	PS

Furthermore, the FOPID controller gives the control system access to fractional-order calculus, which enables more complex and adaptive control responses. Compared to traditional PID controllers, the fractional-order components allow the controller to respond more accurately and efficiently to the dynamic nature of solar resources, as well as subtle variations in water demand. Additionally, the GTO technique is used to optimize the O-FFOPID controller. Through this optimization process, the fuzzy-FOPID controller's parameters are adjusted to optimize the system's energy extraction from renewable sources and maintain smooth operation under a variety of load demands and environmental conditions. The O-FFOPID controller is an extensive and sophisticated control strategy that dynamically regulates power flow in a water pumping system by utilizing fuzzy logic, fractional-order calculus, and optimization techniques. The O-FFOPID controller enhances overall system performance, reliability, and sustainability by intelligently adjusting the BLDC motor's speed and power consumption based on changing environmental conditions and water demand. This ensures efficient utilization of energy from renewable sources.

4. Result and Discussion

A PV array, wind energy, and a 180-volt grid acting as a backup power source are some of the sources of power used to power a motor in the proposed scheme, which is carefully examined through MATLAB-based Simulink simulations. Different scenarios are taken into account, including those in which the PV array is the only source of power, in which the grid is the only source of power and in which there are transitions between these various operating conditions. These simulations allow for a thorough investigation of the system's steady-state, starting, and dynamic responses. The PV voltage and current are shown in Figures 5(a) and (b).

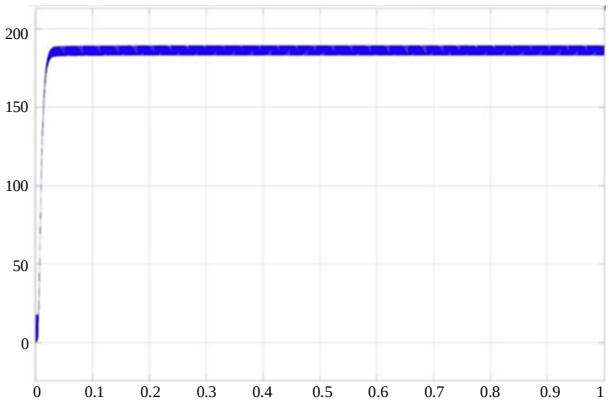

Fig. 5(a) PV voltage

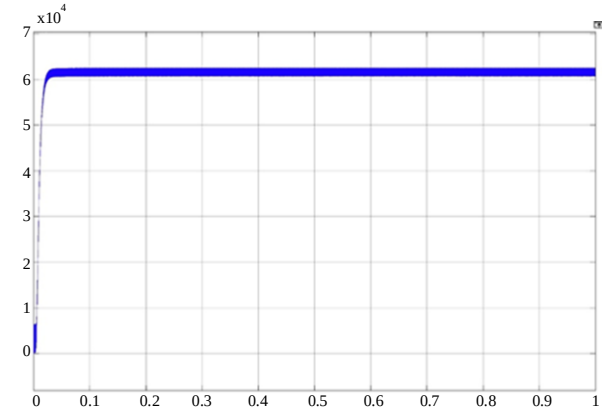

Fig. 5(b) PV current

4.1. Starting and Steady State Response

The motor's soft starting response is shown, illustrating how it gradually increases speed and power consumption during startup instead of experiencing abrupt surges or jolts. This soft starting response extends the life and reliability of the motor and other components by reducing stress on them in their entirety. In this case, the PV array and wind power can produce enough energy, especially when the sun is shining fully, to meet the system's entire water delivery needs without the assistance of the utility.

Ample energy availability is ensured by the specified radiation of 1000 W/m^2 and 10 kW of wind power. The PV array is specifically intended to produce 1.5 kWp of power. In situations where radiation levels fall below the maximum value (e.g., 800 W/m^2) but wind power stays at 10 kW, the PV array might not produce enough power to meet the entire water delivery requirement. To make up for the PV generation shortfall in such circumstances, the system might have to rely more on wind power.

In contrast, the PV array takes over as the main energy source, and its contribution rises to make up for the drop in wind power if radiation stays at 1000 W/m^2 but wind power drops to 5 kW. To maintain efficient water delivery, the system dynamically modifies the power distribution. Figure 6 depicts the steady state response of the BLDC motor.

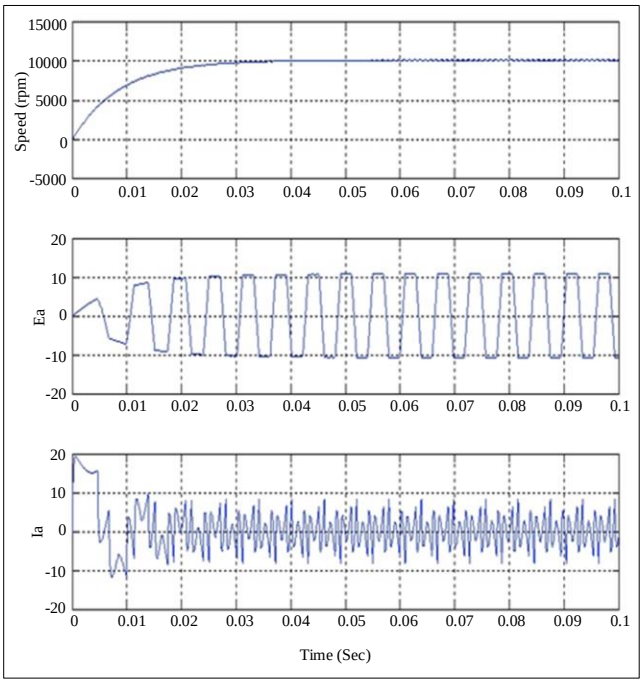

Fig. 6 Steady-state and starting performance of BLDC motor pump

4.2. Dynamic Response of the PV

The proposed approach is made to react dynamically and robustly to variations in operating conditions. This flexibility is essential for sustaining steady performance and guaranteeing dependable operation, especially when reacting to variations in the climate or the status of the grid. The system automatically modifies its power intake from the utility grid in situations where weather conditions change, such as variations in solar radiation.

The system may take full power, a portion of the power, or no power at all from the utility grid, depending on the amount of solar energy available. When renewable energy sources are available, the system can prioritize using them to maximize energy utilization. When the motor pump needs more power, it can smoothly switch to grid power and meet its demands.

Comparably, in the case of a grid failure, the system completely depends on backup power systems or renewable energy sources to react dynamically to the loss of an external power supply. The system ensures that the motor pump always receives the rated power by continuously regulating the common DC bus voltage, irrespective of the external environment. Dynamic regulation facilitates smooth transitions between various power sources and operational states, thereby preserving stability and dependability in the system's operation. Figure 7 shows the dynamic response of the PV.

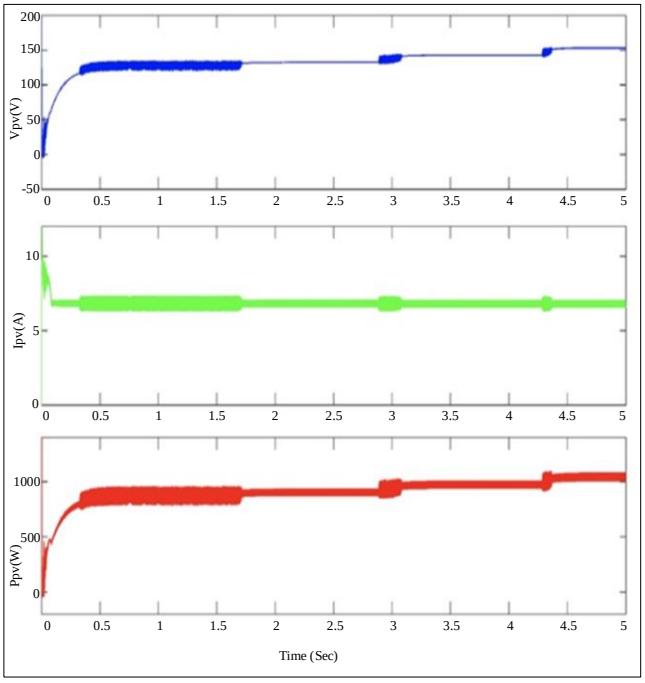

Fig. 7 Dynamic response of the PV

This scenario simulates a sudden change in solar radiation from 300 to 1000 W/m^2. The motor pump gets its rated power from the solar array and utility grid before this switch. This indicates that to keep the motor pump running at the appropriate power level, the system is pulling power from both sources. The PV array can produce its maximum power after the transition, though, because the Maximum Power Point (MPP) is tracked as solar radiation rises until it reaches its maximum value.

The system's power flow control mechanism forbids current from leaving the utility grid. As a result, the pump is completely driven by the PV array and no longer draws grid current. The pump maintains its rated speed throughout the transition and change in power source. This is accomplished by controlling the power flow from the PV array, which guarantees that the motor will always have access to the power it needs to run at its rated speed, even when solar radiation levels fluctuate.

In this case, after the transition, the radiation level returns to 300 W/m^2. However, the system's power flow control mechanism modifies itself as the radiation drops to 300 W/m^2. It permits the necessary amount of power to be transferred to the DC bus to compensate for the PV array's decreased power generation. To guarantee that the motor pump keeps getting the power it needs to run at maximum

efficiency, this adjustment is required. The motor pump's speed and current remain at their rated values despite the power redistribution and source changes. This is accomplished by carefully regulating the power flow and dynamically adjusting the system's operation to guarantee that the motor pump will always run reliably and effectively, regardless of the changes in the surrounding environment.

4.3. Grid Feeds to the Motor

The motor only uses the utility grid to provide the necessary power throughout the night when solar radiation is not present. Under these conditions, the system maintains a unity power factor while obtaining a sinusoidal current at a peak value of 10.64 A from the grid to guarantee that the motor runs effectively. Thus, the motor uses the grid's current in a way that maximizes the phase relationship between the voltage and current, minimizing reactive power consumption and enabling effective power transfer.

Additionally, the system preserves 270 V DC bus power while acquiring power from the utility grid. To prevent voltage fluctuations that might reduce efficiency or harm the equipment, voltage regulation is necessary to guarantee steady operation of the motor and other parts linked to the DC bus. Through the regulation of the DC bus voltage and the maintenance of a sinusoidal current at unity power factor, the system maximizes energy efficiency and guarantees the motor pump's dependable operation at night. The outcomes of BLDC fed by the utility grid are depicted in Figure 8.

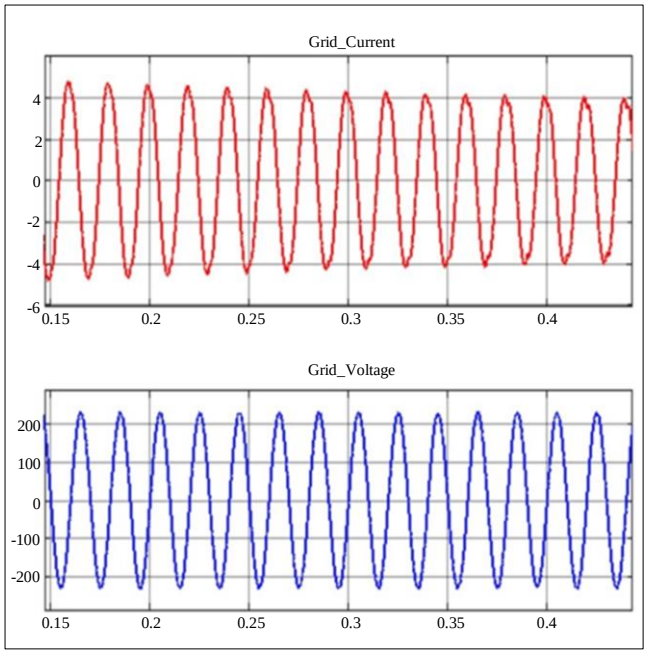

Fig. 8 Utility grid feeds BLDC motor

4.4. Power Quality Aspects

The amount of distortion in a signal relative to its fundamental frequency component is measured by its THD. THD measures the amount of harmonic distortion in the voltage or current waveform. When non-linear loads introduce frequencies into the electrical system that are multiples of the fundamental frequency, harmonic distortion results. To ensure smooth operation and avoid damage to connected electrical equipment, maintaining good power quality is crucial in the proposed system, which uses power from both the utility grid and a PV-wind system to operate the water pump.

To evaluate power quality, the distribution of harmonic components in the current waveform is represented by the harmonic spectrum of the grid current. Good power quality is indicated by a low THD value, which shows that the harmonic distortion in the grid current is negligible. Figure 9 shows the THD analysis.

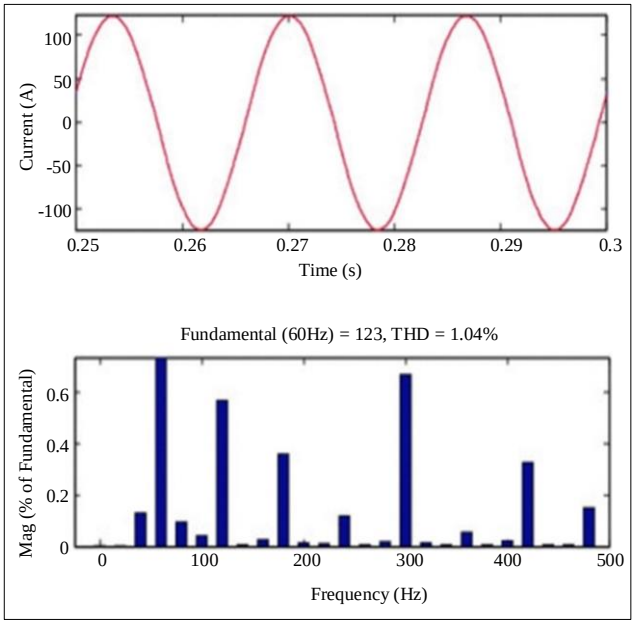

Fig. 9 THD when the PV-wind system and utility grid are both feeding the water pump

The proposed system maintains good power quality and uses power from both the utility grid and a PV-wind system. This is demonstrated by the grid current's harmonic spectrum, which has a low THD of 1.04%. The water pumping system operates smoothly, and connected electrical equipment is shielded from any negative effects thanks to the preservation of power quality.

5. Conclusion

This study offered a novel approach to hybrid energy system optimization that combines grid-controlled photovoltaic power and wind energy with a brushless DC motor for water-pumping applications. For step size optimization, the suggested method combines the INC-GTO MPPT algorithm with GTO, guaranteeing effective power extraction from renewable sources. Furthermore, a GTO-optimized O-FFOPID controller dynamically modifies the

speed and power consumption of the BLDC motor in response to changes in water demand and environmental factors. The study illustrates the system's capacity to achieve MPP operation for the PV array and enhance power quality, including reduced THD in the grid and power factor correction, using MATLAB-based Simulink simulations. The proposed system maintains good power quality with a low THD of 1.04% in the grid current during switches from solar to grid power. System sustainability and reliability are improved by integrating renewable energy sources with innovative optimization techniques and adaptive control strategies. The outcomes demonstrate how well the proposed approach works to maximize energy extraction from renewable sources while maintaining power quality and facilitating seamless operation. The system shows its potential for useful application in water pumping systems, especially in remote or off-grid locations, by making full use of the PV array, wind energy, and grid backup power.

References

[1] Mulugeta Tadesse, and Chernet Merkneh, "Design of Solar PV Underground Water Pumping System for Household Water Consumption in Bilate Basin, Ethiopia," *International Journal of Engineering Trends and Technology*, vol. 68, no. 2, pp. 49-56, 2020. [CrossRef] [Google Scholar] [Publisher Link]

[2] Moses Jeremiah Barasa Kabeyi, and Oludolapo Akanni Olanrewaju, "Sustainable Energy Transition for Renewable and Low Carbon Grid Electricity Generation and Supply," *Frontiers in Energy Research*, vol. 9, pp. 1-45, 2021. [CrossRef] [Google Scholar] [Publisher Link]

[3] Imad H. Ibrik, "Techno-Economic Feasibility of Energy Supply of Water Pumping in Palestine by Photovoltaic Systems, Diesel Generators and Electric Grid," *International Journal of Energy Economics and Policy*, vol. 10, no. 3, pp. 69-75, 2020. [Google Scholar] [Publisher Link]

[4] Atarsia Loubna, Toufouti Riad, and Meziane Salima, "Standalone Photovoltaic Array FED Induction Motor Driven Water Pumping System," *International Journal of Electrical and Computer Engineering*, vol. 10, no. 5, pp. 4534-4542, 2020. [CrossRef] [Google Scholar] [Publisher Link]

[5] Anshul Varshney, Utkarsh Sharma, and Bhim Singh, "An Intelligent Grid-Integrated Solar PV Array FED RSM Drive-Based Water Pumping System," *IEEE Transactions on Industry Applications*, vol. 57, no. 2, pp. 1818-1829, 2021. [CrossRef] [Google Scholar] [Publisher Link]

[6] Alessandro Miglioli et al., "Photovoltaic-Thermal Solar-Assisted Heat Pump Systems for Building Applications: Integration and Design Methods," *Energy and Built Environment*, vol. 4, no. 1, pp. 39-56, 2023. [CrossRef] [Google Scholar] [Publisher Link]

[7] Shreekara S. Hegde, and A.N. Nagashree, "Enhancement of Power Quality and Speed Regulation of a BLDC Motor Drive Using Water Cycle Algorithm," *International Journal of Innovative Science and Research Technology*, vol. 5, no. 8, pp. 541-550, 2020. [CrossRef] [Google Scholar] [Publisher Link]

[8] Bahadur Singh Pali, and Shelly Vadhera, "A Novel Approach for Hydropower Generation Using Photovoltaic Electricity as Driving Energy," *Applied Energy*, vol. 302, 2021. [CrossRef] [Google Scholar] [Publisher Link]

[9] D. Prakasa Rao et al., "A Vector Control Theory Applied in a Grid Connected BLDC Drive with PV with Advanced MPPT Support," *International Journal of Advanced Research in Science & Technology*, vol. 13, no. 4, pp. 197-205, 2020. [Google Scholar]

[10] Ali M. Eltamaly, Zeyad A. Almutairi, and Mohamed A. Abdelhamid, "Modern Optimization Algorithm for Improved Performance of Maximum Power Point Tracker of Partially Shaded PV Systems," *Energies*, vol. 16, no. 13, pp. 1-22, 2023. [CrossRef] [Google Scholar] [Publisher Link]

[11] Niranjan Kumar, and Rahul Malviya, "Advanced MPPT Controller PVA Connected Grid System for BLDC Motor Drive," *International Journal of Innovative Research in Technology and Management*, vol. 4, no. 1, pp. 46-53, 2020. [Google Scholar] [Publisher Link]

[12] Mohammed Benzaouia et al., "Energy Management Strategy for Optimum Control of A Standalone Photovoltaic-Batteries Water Pumping System for Agriculture Applications," *Proceedings of the 2nd International Conference on Electronic Engineering and Renewable Energy Systems*, pp. 855-868, 2020. [CrossRef] [Google Scholar] [Publisher Link]

[13] Fatima Belgacem et al., "Optimization of Photovoltaic Water Pumping System Based on BLDC Motor for Agricultural Irrigation with Different MPPT Methods," *PeriodicaPolytechnica Electrical Engineering and Computer Science*, vol. 66, no. 4, pp. 315-324, 2022. [CrossRef] [Google Scholar] [Publisher Link]

[14] Surabhi Chandra, Prerna Gaur, and Diwaker Pathak, "Radial Basis Function Neural Network Based Maximum Power Point Tracking for Photovoltaic Brushless DC Motor Connected Water Pumping System," *Computers & Electrical Engineering*, vol. 86, 2020. [CrossRef] [Google Scholar] [Publisher Link]

[15] Hamza Alrajoubi, Selim Oncu, and Sinan Kivrak, "An MPPT-Controlled BLDC Motor Driven Water Pumping System," *2021 10th International Conference on Renewable Energy Research and Application (ICRERA)*, Istanbul, Turkey, pp. 116-119, 2021. [CrossRef] [Google Scholar] [Publisher Link]

[16] Bairu Kishore, and V. Prashanth, "Grid Interactive Solar PV Based Water Pumping Using Bldc Motor Drive," *Journal of Engineering Sciences*, vol. 13, no. 10, pp. 90-99, 2022. [Publisher Link]

[17] P.V.V. Satyanarayana, and A. Arun Kumar, "Photovoltaic Based Landsman Converter with Fuzzy Logic Controller FED BLDC Motor for Water Pumping Applications," *International Journal for Advanced Research in Science and Technology*, vol. 11, no. 8, pp. 182-191, 2021. [Google Scholar]

[18] Sabah Miqoi, Abdelghani El Ougli, and Belkassem Tidhaf, "Adaptive Fuzzy Sliding Mode Based MPPT Controller for a Photovoltaic Water Pumping System," *International Journal of Power Electronics and Drive Systems*, vol. 10, no. 1, pp. 414-422, 2019. [CrossRef] [Google Scholar] [Publisher Link]

[19] Tingting Wang et al., "A Novel PID Controller for BLDCM Speed Control Using Dual Fuzzy Logic Systems with HSA Optimization," *Scientific Reports*, vol. 12, pp. 1-19, 2022. [CrossRef] [Google Scholar] [Publisher Link]

[20] Ghasem Shokri, Elahe Naderi, and Mohsen Najafpour, "DTC Based BLDC Motor Controlled Centrifugal Pump FED by PI-BFO Tuning Strategy for Buck-Boost Converter in Solar PV Array Water Pumping System," *2019 10th International Power Electronics, Drive Systems and Technologies Conference (PEDSTC)*, Shiraz, Iran, pp. 769-774, 2019. [CrossRef] [Google Scholar] [Publisher Link]

[21] Ihor Shchur, Marek Lis, and Yurii Biletskyi, "Passivity-Based Control of Water Pumping System Using BLDC Motor Drive FED by Solar PV Array with Battery Storage System," *Energies*, vol. 14, no. 23, pp. 1-25, 2021. [CrossRef] [Google Scholar] [Publisher Link]

[22] André de Oliveira Ferreira et al., "Modeling, Control and Simulation of a Small Photovoltaic-Wind Water Pumping System without a Battery Bank," *Computers & Electrical Engineering*, vol. 84, 2020. [CrossRef] [Google Scholar] [Publisher Link]

[23] Hale Bakır, Adel Merabet, and Mohammadali Kiehbadroudinezhad, "Optimized Control of a Hybrid Water Pumping System Integrated with Solar Photovoltaic and Battery Storage: Towards Sustainable and Green Water-Power Supply," *Energies*, vol. 16, no. 13, pp. 1-16, 2023. [CrossRef] [Google Scholar] [Publisher Link]

[24] Saurabh Shukla, and Bhim Singh, "Single-Stage PV-Grid Interactive Induction Motor Drive with Improved Flux Estimation Technique for Water Pumping with Reduced Sensors," *IEEE Transactions on Power Electronics*, vol. 35, no. 12, pp. 12988-12999, 2020. [CrossRef] [Google Scholar] [Publisher Link]

[25] E. Ramakrishna et al., "ANFIS Based Grid Connected Solar PV Based Water Pumping Using BLDC Motor Drive," *Industrial Engineering Journal*, vol. 52, no. 4, pp. 2293-2298, 2023. [Publisher Link]